

Electrically tunable spin-orbit coupled photonic lattice in a liquid crystal microcavity – Supplementary Information

Marcin Muszyński,¹ Przemysław Oliwa,¹ Pavel Kokhanchik,² Piotr Kapuściński,¹ Eva Oton,³
Rafał Mazur,³ Przemysław Morawiak,³ Wiktor Piecek,³ Przemysław Kula,⁴ Witold Bardyszewski,⁵
Barbara Piętko,¹ Daniil Bobylev,² Dmitry Solnyshkov,^{2,6} Guillaume Malpuech,² and Jacek Szczytko¹

¹*Institute of Experimental Physics, Faculty of Physics, University of Warsaw, Poland*

²*Université Clermont Auvergne, Clermont Auvergne INP,
CNRS, Institut Pascal, F-63000 Clermont-Ferrand, France*

³*Institute of Applied Physics, Military University of Technology, Warsaw, Poland*

⁴*Institute of Chemistry, Military University of Technology, Warsaw, Poland*

⁵*Institute of Theoretical Physics, Faculty of Physics, University of Warsaw, Poland*

⁶*Institut Universitaire de France (IUF), 75231 Paris, France*

I. BAND STRUCTURE EXPLAINED THROUGH DIRECTOR DISTRIBUTION

A. Sample A

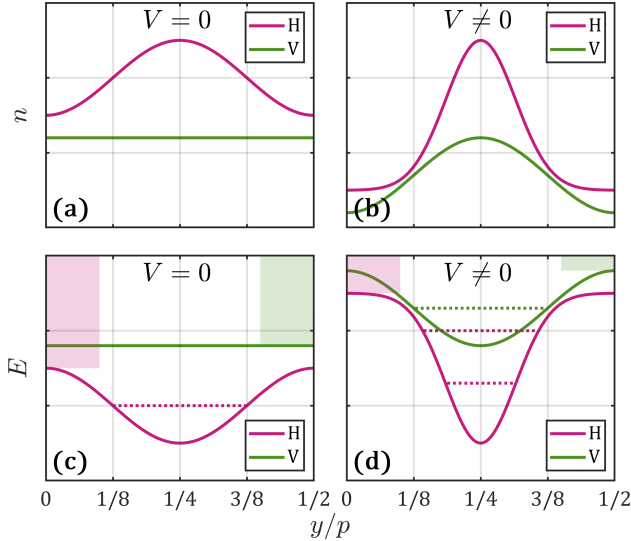


FIG. S1 Schematic dependence of refractive indices and corresponding potentials for sample A. Refractive index real space dependence for (a) zero and (b) non-zero voltage. Resulting periodic potentials for (c) zero and (d) non-zero voltage. Pink and green colors correspond to H and V polarizations, respectively. Dotted lines show localized states and colored rectangles show the energy range of the continuum.

The dynamics of the dispersion under an applied electric field can be carefully explained using the director distributions shown in Fig. 2a,b of the main text. The ideal helix creates a perfectly uniform distribution of the director along the microcavity axis z . Its projection on microcavity plane x - y shows a periodic variation of refractive index along y for one polarization (H) and the absence of variation for another polarization (V). In real-

ity, the helix is not ideal, and the angular fluctuations [1] of molecules from ideal orientation occur. Under zero electric field, these deviations are randomly distributed and do not have any preferential direction. In general, their effect is a reduction of the effective refractive index contrast. In other words, if we now average the LC director distribution along z taking into account these fluctuations (Fig. 2a of the main text), the maximum (minimum) refractive index is reduced (increased) for both polarizations in comparison to the ideal helix. The result of this averaging is shown in Fig. 2c of the main text in the form of effective refractive index ellipses for H and V polarizations. It is also shown in a more standard way in Fig. S1a, as two separate functions, n_H (pink) and n_V (green), representing the effective refractive indices for H and V polarization, respectively. The polarization-dependent potentials created by these refractive index distributions are calculated as:

$$V_{H,V} = \frac{\pi \hbar c N}{n_{H,V} L} \propto \frac{1}{n_{H,V}}, \quad (\text{S1})$$

with reduced Planck constant \hbar , speed of light c , microcavity mode number N , and microcavity length L . These potentials are schematically depicted in Fig. S1c. The periodic potential with half-pitch period $p/2$ is present for H and absent for V . Naturally, if the potential for H is deep enough, it contains a localized state (shown as a dotted line in Fig. S1c), exactly as in the experiment (Fig. 2e of the main text).

When the voltage is applied to the cavity along the z axis, molecules aligned closely to the electric field direction are the first to react on the field, and they realign with it even better, while molecules perpendicular to the field almost do not realign. This effect is often referred to as the dielectric effect of the electric field [2]]. Thus, the uniformization of the director distribution along z happens for some regions (edges of the distribution in Fig. 2b,d of the main text, $y/p \approx 0$ or $1/2$), while it does not happen for the others (middle of the distribution in Fig. 2b,d of the main text, $y/p \approx 1/4$). Therefore, the effective refractive index contrast is increasing for both polarizations: the highest refractive indices for H and V stay the same, while the lowest ones are decreasing,

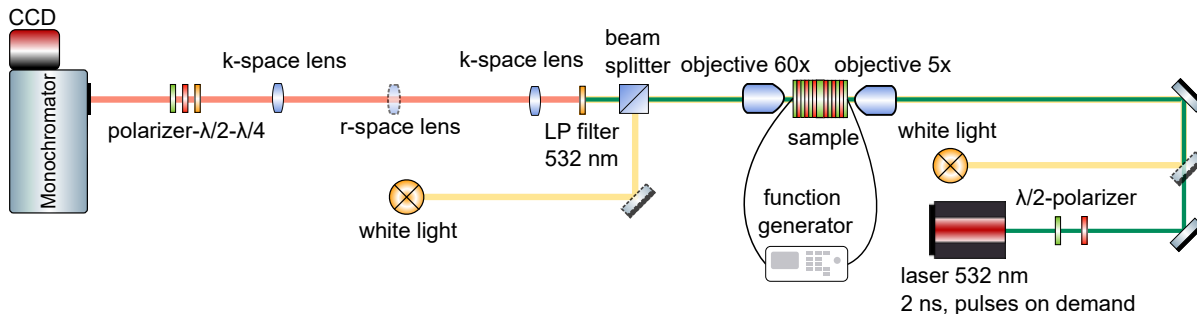


FIG. S2 Scheme of the experimental optical setup.

as shown in Fig. S1b. Also, the narrowing of the central region (high refractive index region) happens (more red-colored directors appear in Fig. 2b of the main text with respect to Fig. 2a of the main text). In complete analogy with zero voltage case, the potential is calculated by Eq. (S1) and shown in Fig. S1d. Now, the potential appears for V polarization, with a localized state inside. For H polarization, the potential deepens and allows now for two localized states. The continuum of states for both H and V is also shifted towards higher energy (shown by the pink and green colored rectangles, respectively). The described qualitative behavior agrees perfectly with the experimental observations presented in Fig. 2e-j of the main paper.

B. Sample B

Although it is well known that the helix of CLC creates the OA in an unbounded medium [3], in our case, the OA is due to the combination of molecular tilt and helix, and not due to the helix alone. This can be explained from the point of view of system symmetry. The unbounded medium with a cholesteric helix does not show the inversion symmetry. This leads to the emergence of OA. When a cholesteric helix is bounded by the cavity in the ULH configuration, it can be unfolded to pave the space by building the reflection of the helix in the mirrors. In this case, the inversion symmetry (up to a supplementary translation by cavity width) is restored, preventing the appearance of OA. That is why the helix-induced OA does not show up in sample A (see Fig. 2 of the main paper). Finally, when a tilt is introduced, the inversion symmetry is broken again (along x), and OA is restored. That is what happens in sample B giving rise to the s - p band hybridization.

II. EXPERIMENT

Figure S2 presents the optical experimental setup described in detail in the Methods section of the main text. Depending on the selected lenses (k -space or r -space) and the light source, the setup allows measuring the recipro-

cal space (reflectivity of white light and photoluminescence), as well as the real space (transmission of white light) at the same position on the sample. Paths of white light are indicated by yellow lines, laser light paths are marked with green lines, and the signal from the sample is represented by an orange line.

Fig. S3 shows the Stokes parameter S_3 for angular-resolved reflectivity spectra measured at different positions on sample B. The positions were selected to have different detunings between the mixed ISOC states. It can be seen that with increasing detuning, the degree of circular polarization of mixed states decreases.

Fig. S4 shows the emission intensity (panel a) and full width at half maximum (panel b) of the two lowest ULH states (H_s and the ISOC-mixed state) as a function of the excitation laser pulse energy measured for sample B. The values were obtained by fitting with a Gaussian curve the polarization- and momentum-integrated photoluminescence spectra. For a pulse energy of 0.36 μJ , a clear lasing threshold is observed, above which the emission intensity of both states exhibits an abrupt increase and the widths of both spectral lines undergo a significant narrowing. Competition between the two lasing states is also present, where, above the threshold, the emission intensities fluctuate.

III. SOLUTION OF MAXWELL'S EQUATIONS BASED ON A FINITE ELEMENT METHOD

To get a deeper insight into physical mechanisms governing the observed effects, a series of numerical simulations was performed using COMSOL Multiphysics® software. The 2D (yz) simulations were based on the Electromagnetic Waves, Frequency Domain Physics Interface of the Wave Optics Module and the Eigenfrequency Study. The computational domain is represented by a unit cell consisting of: (i) the microcavity domain of height $a_0 = 2 \mu\text{m}$ corresponding to the ULH period and width $t_0 = 200 \text{ nm}$ corresponding to the effective microcavity thickness; (ii) the out-of-microcavity domains of width $s_0 = 160 \text{ nm}$ each. The Layered Transition Boundary Condition is applied to the boundaries separating the regions inside and outside the microcavity; the number

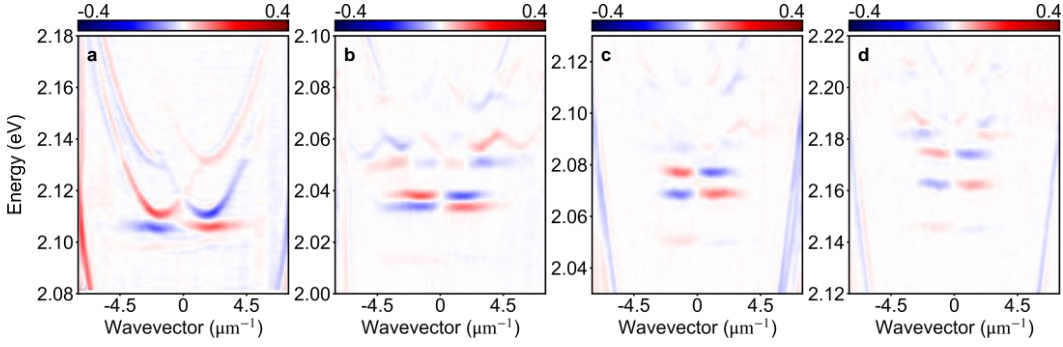


FIG. S3 Degree of circular polarization expressed by Stokes parameter S_3 for different detunings between ISOC-mixed states. (a-d) Angle-resolved reflectivity spectra measured for different positions on sample B.

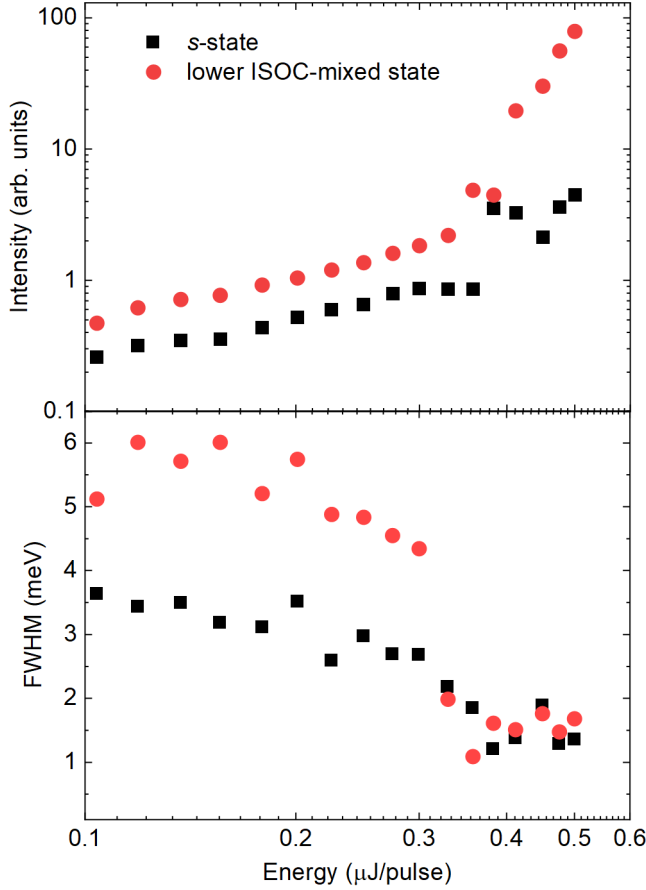


FIG. S4 (a) Intensity and (b) full width at half maximum as a function of pumping pulse energy for horizontally polarized s -state and ISOC-mixed state.

of layers is set to 11, where the first one has refractive index $n_{\text{TiO}_2} = 2.436$, the second one has $n_{\text{SiO}_2} = 1.456$, and the subsequent layers alternate. Their thicknesses $t_{\text{TiO}_2/\text{SiO}_2}$ are tuned so $t_{\text{TiO}_2/\text{SiO}_2} = \lambda_0/(4n_{\text{TiO}_2/\text{SiO}_2})$, where $\lambda_0 = 550$ nm. The Floquet Periodic Boundary Condition is applied to the top and the bottom boundaries of the computational domain, whereas the Scatter-

ing Boundary Condition was applied to the side boundaries. The Scattering Boundary Condition is automatically tuned to the frequency searched around in the Eigenfrequency Study, which was set to 5×10^{14} Hz (≈ 2.07 eV). Due to the system's rectangular symmetry, the Mapped Mesh was used everywhere.

The regions outside the microcavity have relative permittivity $\varepsilon = 1$, relative permeability $\mu = 1$ and conductivity $\sigma = 0$. The region inside the microcavity has relative permeability $\mu = 1$, conductivity $\sigma = 0$ and relative permittivity defined as $\varepsilon_{\alpha,\beta} = n_o^2 \delta_{\alpha,\beta} + (n_e^2 - n_o^2) \hat{r}_\alpha \hat{r}_\beta$, where $n_o = 1.775$, $n_e = 1.825$, $\hat{r}_\alpha, \hat{r}_\beta$ are the $\alpha = x, y, z$ and $\beta = x, y, z$ components of the liquid crystal director \hat{r} , and $\delta_{\alpha,\beta}$ is the Kronecker symbol. The director \hat{r} is defined as

$$\hat{r} = \mathbf{R}_x(\alpha_x) \mathbf{R}_y(\alpha_y(y)) \hat{r}^{(0)}, \quad (\text{S2})$$

where

$$\hat{r}^{(0)} = \begin{bmatrix} 0 \\ 0 \\ 1 \end{bmatrix}, \quad (\text{S3a})$$

$$\mathbf{R}_x(\alpha_x) = \begin{bmatrix} 1 & 0 & 0 \\ 0 & \cos(\alpha_x) & -\sin(\alpha_x) \\ 0 & \sin(\alpha_x) & \cos(\alpha_x) \end{bmatrix}, \quad (\text{S3b})$$

$$\mathbf{R}_y(\alpha_y(y)) = \begin{bmatrix} \cos(\alpha_y(y)) & 0 & \sin(\alpha_y(y)) \\ 0 & 1 & 0 \\ -\sin(\alpha_y(y)) & 0 & \cos(\alpha_y(y)) \end{bmatrix}. \quad (\text{S3c})$$

Here, the angle $\alpha_y(y) = \pi y/a_0$ is responsible for the ULH formation, whereas the angle α_x is responsible for the molecules' tilt.

The obtained simulation results are represented by spatial distributions of the electric field Cartesian components $E_{x,y,z}$ corresponding to the found 32 eigenfrequencies for each of 51 considered Bloch wavenumbers. For

the first five modes of interest derived by filtering the eigenfrequencies, periodic parts of E_x and E_y were calculated at 2^6 points along a line parallel to the microcavity mirrors crossing the point $(y, z) = (0.5(t_0 + s_0), 0)$. These periodic parts were duplicated 2^4 times and multiplied by the corresponding Bloch phase; then, the DFT of the obtained sequence of complex numbers was performed. Based on the Fourier images of the extended $E_{x,y}$ the Stokes parameters were calculated in reciprocal space. The results of post-processing for $\alpha_x = 0^\circ, 10^\circ, 20^\circ$ are presented in Fig. S5 proving the necessity of tilt to observe optical activity. It is noteworthy that another tilt angle α_z (rotation around z) does not give optical activity along k_y .

IV. TIGHT-BINDING MODEL

In the simplest approximation, the potential created by ULH (Figs. 2a and 3a of the main text) for each polarization can be described as a cosine function: $U_{H,V}(y) = 0.5A_{H,V} \cos(2qy)$, where $A_{H,V}$ are the potential amplitudes for H and V , $q = 2\pi/p$, and p is the pitch of the ULH. When the tilt is present in a stable molecular director distribution, these linear polarizations are coupled.

This coupling can be well described by introducing a SOC between linear polarizations proportional to the wavevector k_y , which reads in (H, V) basis as $-2i\alpha\sigma_x\partial_y$, with the SOC amplitude α and the first Pauli matrix σ_x . This SOC is equivalent to the OA in the regime of small in-plane wavevectors k_y with respect to $q/\Delta n$. As OA, it appears due to the inversion symmetry breaking in the system. The SOC amplitude α is an energy-dependent function in general, but since we are aiming to reproduce only H_p and V_s band coupling, we can consider it to be a constant. Then, the Hamiltonian of the tilted ULH, including SOC (OA), can be written in (H, V) basis in real space as:

$$H_{cont} = \begin{pmatrix} -\frac{\hbar^2}{2m} \frac{\partial^2}{\partial y^2} + \frac{A_H}{2} [1 - \cos(2qy)] - \frac{\delta}{2} & -2i\alpha \frac{\partial}{\partial y} \\ -2i\alpha \frac{\partial}{\partial y} & -\frac{\hbar^2}{2m} \frac{\partial^2}{\partial y^2} + \frac{A_V}{2} [1 - \cos(2qy)] + \frac{\delta}{2} \end{pmatrix}, \quad (S4)$$

with \hbar reduced Planck constant, m mass of photon in LC microcavity, and δ detuning between H and V potentials. Since we would like to reproduce the band and polarization structure of low-energy bands H_p and V_s well-isolated from other bands, we can reduce the Hamiltonian (S4) to two-band tight-binding Hamiltonian. The cosine potential of each polarization can

be well-approximated by harmonic oscillator potential for lower energy states, which allows us to use s and p eigenstates of a harmonic oscillator as basis states $|0(y), V\rangle$ and $|1(y), H\rangle$, respectively. Thus, the tight-binding Hamiltonian of ULH, including ISOC, writes in k -space as:

$$H = \begin{pmatrix} E_{H_p} - 2t_{pp} \cos(k_y p/2) & -i\alpha [t_{sp,0} - 2t_{sp,1} \cos(k_y p/2)] \\ c.c. & E_{V_s} - 2t_{ss} \cos(k_y p/2) \end{pmatrix}, \quad (S5a)$$

$$E_{H_p} = \langle 1(y), H | \left(-\frac{\hbar^2}{2m} \frac{\partial^2}{\partial y^2} + \frac{A_H}{2} [1 - \cos(2qy)] - \frac{\delta}{2} \right) | 1(y), H \rangle, \quad (S5b)$$

$$E_{V_s} = \langle 0(y), V | \left(-\frac{\hbar^2}{2m} \frac{\partial^2}{\partial y^2} + \frac{A_V}{2} [1 - \cos(2qy)] + \frac{\delta}{2} \right) | 0(y), V \rangle, \quad (S5c)$$

$$t_{pp} = \langle 1(y + p/2), H | \left(-\frac{\hbar^2}{2m} \frac{\partial^2}{\partial y^2} + \frac{A_H}{2} [1 - \cos(2qy)] - \frac{\delta}{2} \right) | 1(y), H \rangle, \quad (S5d)$$

$$t_{ss} = \langle 0(y + p/2), V | \left(-\frac{\hbar^2}{2m} \frac{\partial^2}{\partial y^2} + \frac{A_V}{2} [1 - \cos(2qy)] + \frac{\delta}{2} \right) | 0(y), V \rangle, \quad (S5e)$$

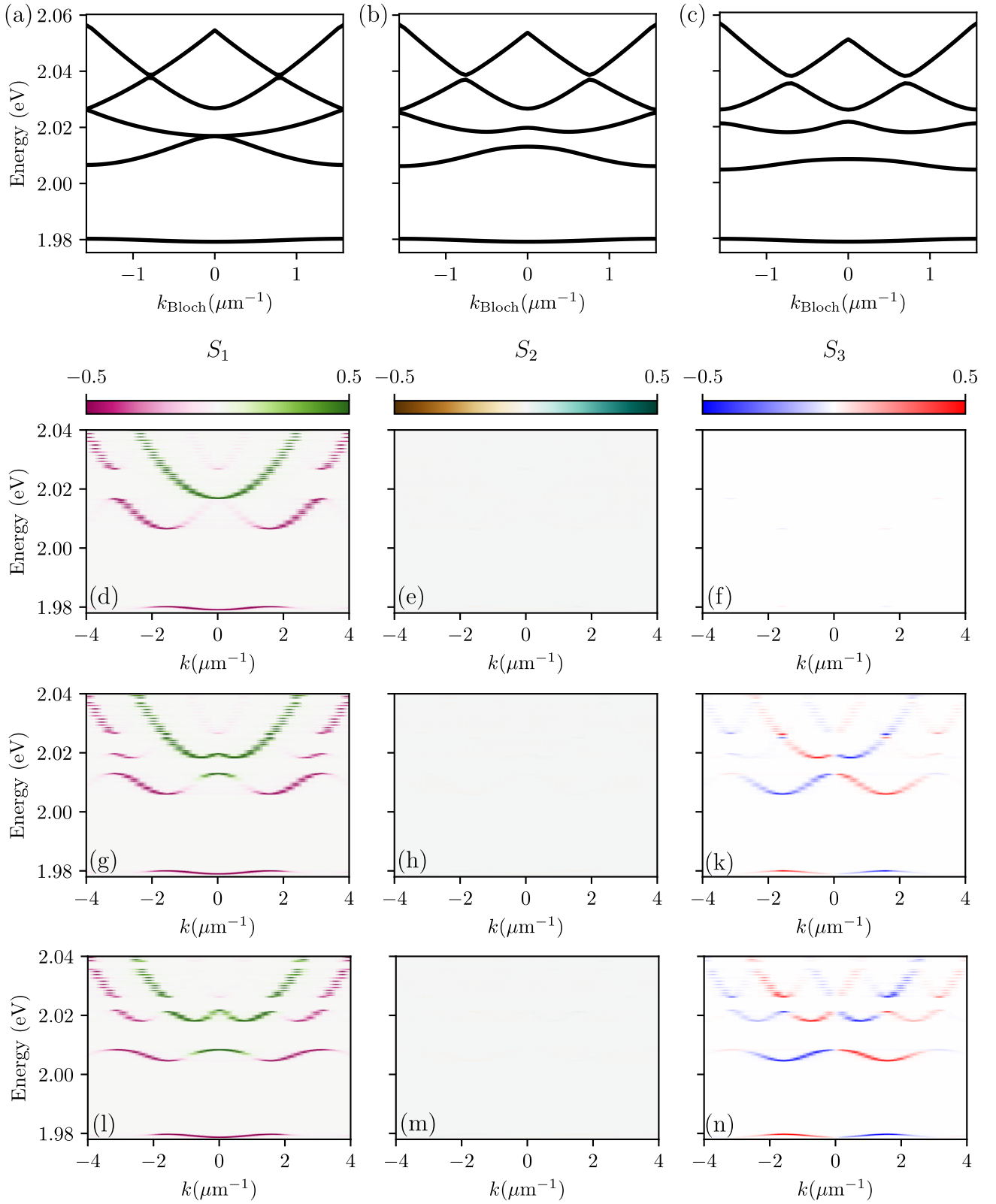


FIG. S5 Simulation results. (a,b,c) Band structures for $\alpha_x = 0^\circ, 10^\circ, 20^\circ$, respectively. (d-f), (g-k), (l-n) S_{1-3} Stokes parameter corresponding to the first 5 eigenenergies in reciprocal space for $\alpha_z = 0^\circ, 10^\circ, 20^\circ$, respectively.

$$t_{sp,0} = \langle 1(y), H | 2\partial_y | 0(y), V \rangle, \quad (\text{S5f})$$

$$t_{sp,1} = \langle 1(y + p/2), H | 2\partial_y | 0(y), V \rangle, \quad (\text{S5g})$$

with E_{H_p} and E_{V_s} onsite energies of H_p and V_s , respectively, t_{pp} and t_{ss} nearest-neighbour couplings between p states of H and s states of V , respectively, $t_{sp,0}$ and $t_{sp,1}$ onsite and nearest-neighbour couplings between H_p and V_s , respectively. The ISOC terms $t_{sp,0}$ and $t_{sp,1}$ can only couple modes of different parity (s and p , for example) since the SOC (OA) is an odd function of k_y . The ISOC onsite coupling $\alpha t_{sp,0}$ is dominant over other coupling terms (t_{pp} , t_{ss} , $\alpha t_{sp,1}$), which is confirmed by efficient mixing of polarizations (high S_3 values in Fig. 3i of the main text), and large band splitting with respect to the band size. The parameters used for Fig. 3b,c of the main text: $E_{H_p} = 24.24$ meV, $E_{V_s} = 23.27$ meV, $t_{pp} = 0.12$ meV, $t_{ss} = 0.10$ meV, $\alpha = 1.1$ meV $\cdot\mu\text{m}$, $t_{sp,0} = 1.71$ μm^{-1} , $t_{sp,1} = 0.06$ μm^{-1} , $p = 8$ μm .

V. SOLUTION OF MAXWELL'S EQUATIONS BASED ON THE FOURIER DECOMPOSITION OF THE DIELECTRIC TENSOR

A. Dielectric tensor

In our approach, the cavity consists of the two δ -mirrors, which are separated by distance L , and the volume between them is filled by a birefringent material. The full description of the orientation of liquid crystal molecules as a function of position is very complex and can be found by using a method based on the thermodynamic potentials [4, 5]. However, the only crucial dependence in this case is in the y direction (parallel to mirror) and other dependencies can be taken into account in the effective approach. As shown in Fig. 1 of the main text the refractive index periodically changes in the y -direction, so the ij element of the dielectric tensor $\hat{\epsilon}$ can be expressed by expanding it into Fourier series:

$$\epsilon_{ij}(y) = \frac{1}{2} \sum_{n=0}^{\infty} \epsilon_{ij,n} e^{4\pi i n y/d} + \epsilon_{ij,n}^* e^{-4\pi i n y/d} \quad (\text{S6})$$

where $\epsilon_{ij,n}$ is a n -th coefficient in Fourier series, d is a pitch (double period) of structure, and $\epsilon_{ij,-n} = \epsilon_{ij,n}^*$, because ϵ_{ij} is a real function and is a symmetric matrix $\hat{\epsilon} = \hat{\epsilon}^T$, where superscript T denotes the transposition of a matrix. Each element $\epsilon_{ij,n}$ is an effective element, which means that it includes the impact of modulation of the liquid crystal molecular director as a function of position in the z direction. The experimental data shows that the amplitudes of modulations along y are small compared to the refractive indices of the liquid crystal mixture, so it can be treated as a perturbation in calculations. It means that we can split our solution into

two parts. In the first one, we found the expression for the unperturbed case – we took into account only the elements for $n = 0$ from Eq. (S6). In the second part, we find the expression for elements of the interaction matrix for all n of $\hat{\epsilon}$ matrix Eq. (S6).

B. Linear operator

In our approach, the elements of the $\hat{\epsilon}$ matrix depend on the y coordinate, so the band structure can occur only in this direction. But, since the k_x component is crucial to obtain few polarization patterns, we take into account all elements of the wave vector in the plane of the cavity. In addition, the modulation along y is small, so in the zero-order approximation we assume that the electric field in the $x - y$ plane has the same form as in [6], so similarly to this work we define a second-order differential equation for a two-dimensional vector of the electric field:

$$\hat{L}(z; \omega, \mathbf{k}) \mathbf{E} = [(\partial_z - \mathbf{A}^T)(\partial_z - \mathbf{A}) - \mathbf{B} + k_0^2 \mathbf{B}_0] \mathbf{E} = \mathbf{0} \quad (\text{S7})$$

where $k_0 = \omega/c$ and all matrices are equal to $\mathbf{A} = \mathbf{A}_x + \mathbf{A}_y$, $\mathbf{B} = \mathbf{B}_x + \mathbf{B}_y + \mathbf{B}_{xy}$, and:

$$\mathbf{A}_y = -\frac{ik_y}{\epsilon_{zz}} \begin{bmatrix} 0 & 0 \\ \epsilon_{xz} & \epsilon_{yz} \end{bmatrix} \quad (\text{S8a})$$

$$\mathbf{A}_x = -\frac{ik_x}{\epsilon_{zz}} \begin{bmatrix} \epsilon_{xz} & \epsilon_{yz} \\ 0 & 0 \end{bmatrix} \quad (\text{S8b})$$

$$\mathbf{B}_y = \frac{k_y^2}{\epsilon_{zz}} \begin{bmatrix} \epsilon_{zz} & 0 \\ \tilde{\epsilon}_{yx} & \tilde{\epsilon}_{yy} \end{bmatrix} \quad (\text{S8c})$$

$$\mathbf{B}_x = \frac{k_x^2}{\epsilon_{zz}} \begin{bmatrix} \tilde{\epsilon}_{xx} & \tilde{\epsilon}_{xy} \\ 0 & \epsilon_{zz} \end{bmatrix} \quad (\text{S8d})$$

$$\mathbf{B}_{xy} = \frac{k_x k_y}{\epsilon_{zz}} \begin{bmatrix} \tilde{\epsilon}_{yx} & \tilde{\epsilon}_{yy} - \epsilon_{zz} \\ \tilde{\epsilon}_{xx} - \epsilon_{zz} & \tilde{\epsilon}_{xy} \end{bmatrix} \quad (\text{S8e})$$

$$\mathbf{B}_0 = \begin{bmatrix} \tilde{\epsilon}_{xx} & \tilde{\epsilon}_{xy} \\ \tilde{\epsilon}_{xy} & \tilde{\epsilon}_{yy} \end{bmatrix} \quad (\text{S8f})$$

where $\tilde{\epsilon}_{ij} = \epsilon_{ij} - \epsilon_{iz}\epsilon_{zj}/\epsilon_{zz}$. The \mathbf{B}_0 matrix can be split into two parts: \mathbf{B}_0^0 which does not depend on the position and \mathbf{B}_0^1 which depends on position, so:

$$\mathbf{B}_0^0 = \begin{bmatrix} \epsilon_{xx,0} & 0 \\ 0 & \epsilon_{yy,0} \end{bmatrix} \quad (\text{S9a})$$

$$\mathbf{B}_0^1 = \mathbf{B}_0 - \mathbf{B}_0^0 \quad (\text{S9b})$$

Experimental data shows that the $\varepsilon_{xy,0} = \varepsilon_{yx,0} = 0$, so we simplify the formula for matrix \mathbf{B}_0^0 , which yields two separate equations for two orthogonal linear polarizations for the unperturbed case. If these elements are different from zero, before further calculation we find the eigenvectors of matrix \mathbf{B} and rotate the basis by a canonical transformation. In addition, $\varepsilon_{xz,0} = 0$, but $\varepsilon_{yz} \neq 0$ so $\tilde{\varepsilon}_{xx,0} = \varepsilon_{xx,0}$ and $\tilde{\varepsilon}_{yy,0} = \varepsilon_{yy,0} - \varepsilon_{yz,0}^2/\varepsilon_{zz,0}$.

C. Hamiltonian matrix

According to [6] the general expression for the resonant state is given by:

$$\hat{\mathcal{L}}(z, \omega_r, \mathbf{k}) \mathbf{u}_r = \mathbf{0}, \quad (\text{S10a})$$

$$\hat{\mathcal{L}}^\dagger(z, \omega_r, \mathbf{k}) \mathbf{w}_r = \mathbf{0}, \quad (\text{S10b})$$

where ω_r is a resonant frequency and $\mathbf{u}_r, \mathbf{w}_r$ are resonant states for equation and coupled equation, and they are normalized, according to:

$$\frac{1}{c^2} \int_a^b \mathbf{w}_r^T(z) \mathbf{B}_0^0(z) \mathbf{u}_r(z) dz + \frac{in_a^2}{2c^2 k_{zr}} \cdot (\mathbf{w}_r^T(b) + \mathbf{u}_r(b) + \mathbf{w}_r^T(a) + \mathbf{u}_r(a)) = 1 \quad (\text{S11})$$

where $\omega_r^2(\mathbf{k}) = (k_{zr}^2 + k_x^2 + k_y^2) c^2 / n_a^2$ and k_{zr} is a resonant wave vector. Using the $\mathbf{u}_r, \mathbf{w}_r$ resonant state, we define the principal part of Green's function:

$$\mathbf{G}(z, z'; \omega, \mathbf{k}) \approx \frac{\mathbf{u}_r(z) \mathbf{w}_r^T(z')}{2\omega_r(\omega - \omega_r)} \quad (\text{S12})$$

Solving Eq. (S10a) in a general case is very difficult, but it can be done using perturbation theory. Similarly to [6], we split the linear operator $\hat{\mathcal{L}}(z, \omega_r, \mathbf{k})$ into resonant (unperturbed) $\hat{\mathcal{L}}_0$ and perturbed $\hat{\mathcal{L}}'$ parts, where the first has the following form:

$$\hat{\mathcal{L}}_0(z, \omega, \mathbf{k}) = \partial_z^2 + \left(\frac{\omega^2}{c^2} - \frac{k_x^2 + k_y^2}{n_a^2} \right) \mathbf{B}_0^0(z) \quad (\text{S13})$$

with unperturbed resonant solution $\overset{\circ}{\mathbf{u}}_r$ obtained from equation:

$$\hat{\mathcal{L}}_0(z, \overset{\circ}{\omega}_r(0), 0) \overset{\circ}{\mathbf{u}}_r = \mathbf{0} \quad (\text{S14})$$

where $\overset{\circ}{\omega}_r^2(\mathbf{k}) = \overset{\circ}{\omega}_r^2(0) + c^2(k_x^2 + k_y^2)/n_a^2$. The perturbed parts depend on ω and are different from zero for the region between mirrors:

$$\hat{\mathcal{L}}' = \hat{\mathcal{L}} - \hat{\mathcal{L}}_0 = -\mathbf{A}^T \partial_z - \partial_z \mathbf{A} + \mathbf{A}^T \mathbf{A} - \mathbf{B} + \frac{k_x^2 + k_y^2}{n_a^2} \mathbf{B}_0^0 + k_0^2 \mathbf{B}_0^1 \quad (\text{S15})$$

The resonant solution for $\mathbf{k} \neq \mathbf{0}$ can be expressed as a linear combination of unperturbed resonant state $\overset{\circ}{\mathbf{u}}_n$:

$$\mathbf{u}_m(z) = \sum_n \frac{a_{nm}}{\sqrt{\overset{\circ}{\omega}_n(\mathbf{k})}} \overset{\circ}{\mathbf{u}}_n(z) \quad (\text{S16})$$

We used Mittag-Leffler theory and obtained expression for unperturbed $\mathbf{G}_0(z, z'; \omega, \mathbf{k})$ and perturbed $\mathbf{G}(z, z'; \omega, \mathbf{k})$ Green's functions:

$$\mathbf{G}_0(z, z'; \omega, \mathbf{k}) = \sum_m' \frac{\overset{\circ}{\mathbf{u}}_m(z) \overset{\circ}{\mathbf{u}}_m^T(z')}{2\overset{\circ}{\omega}_m(\mathbf{k}) (\omega - \overset{\circ}{\omega}_m(\mathbf{k}))}, \quad (\text{S17a})$$

$$\mathbf{G}(z, z'; \omega, \mathbf{k}) = \sum_m' \frac{\overset{\circ}{\mathbf{u}}_m(z) \overset{\circ}{\mathbf{u}}_m^T(z')}{2\overset{\circ}{\omega}_m(\mathbf{k}) (\omega - \overset{\circ}{\omega}_m(\mathbf{k}))}, \quad (\text{S17b})$$

where the summation is over simple poles associated with the resonant state limited to the poles in the lower half of the complex ω plane, including the pole at zero if exists. To determine the elements of the Hamiltonian matrix, we consider the Dyson formula for $\mathbf{G}(z, z'; \omega, \mathbf{k})$:

$$\mathbf{G}(z, z') = \mathbf{G}_0(z, z') - \int_a^b \mathbf{G}_0(z, z'') \hat{\mathcal{L}}'(z'') \mathbf{G}(z'', z') dz'' \quad (\text{S18})$$

Inserting Eq. (S15) and Eq. (S17) to Eq. (S18), after transformation presented in [6] yields a general eigenvalue problem:

$$\sum_p \mathcal{H}_{mp}(\mathbf{k}) a_p = \omega(\mathbf{k}) a_m \quad (\text{S19})$$

with a non-Hermitian Hamiltonian:

$$\mathcal{H}_{mp} = \overset{\circ}{\omega}_m(\mathbf{k}) \delta_{mp} - \frac{\hat{\mathcal{L}}'_{mp}}{2\sqrt{\overset{\circ}{\omega}_m(\mathbf{k}) \overset{\circ}{\omega}_p(\mathbf{k})}} \quad (\text{S20})$$

where

$$\hat{\mathcal{L}}'_{mp} = \int_a^b \overset{\circ}{\mathbf{u}}_m^T(z'') \hat{\mathcal{L}}'(z'') \overset{\circ}{\mathbf{u}}_p^T(z'') dz'' \quad (\text{S21})$$

In the case under consideration, $\hat{\mathcal{L}}'(z)$ includes the term $k_0^2 \mathbf{B}_0^1$ (see Eq. (S15)), necessitating the solution of a general eigenvalue problem. This scenario is referred to as a quadratic eigenvalue problem (QEP), which can be addressed by applying linearization theory. Within the analyzed energy range, k_0^2 varies only slightly, allowing us to approximate this term as having a constant value in the zeroth order of approximation.

D. Electric field in simple cavity

The coordinate dependence of refractive index in the system has the following form:

$$\tilde{n}_s^2(z) = \Theta(L-z)\Theta(z)(n_s^2 - n_a^2) + n_a^2 - \frac{2\zeta_s c^2}{\omega^2}(\delta(z) + \delta(L-z)) \quad (\text{S22})$$

where n_a is a ambient refractive index outside cavity, $n_s = \sqrt{\varepsilon_{ss,0}}$ denotes the refractive index for $s = H$ (horizontal mode) and $s = V$ (vertical mode), ζ_s is the strength of the δ -mirrors and it depends on polarization, and $\Theta(z)$ is a standard Heaviside step function. In this case, the equation for the electric field for the perpendicular incident wave has the following form:

$$\left(\partial_z^2 + \tilde{n}_s^2(z)\frac{\omega^2}{c^2}\right)\mathbf{E}_s(z) = \mathbf{0} \quad (\text{S23})$$

which is the same as the Eq. (S14) and has following solution:

$$\mathbf{E}_{sm}(z) = \mathbf{E}_{0,sm} \sin(\kappa_{sm}(z - d_{sm})) \quad (\text{S24})$$

with normalization accordingly to Eq. (S11), where κ_{sm} is defined in the implicit equation:

$$\kappa_{sm} = -\frac{i}{L} \ln\left(\frac{1 - i\frac{(n_a+n_s)\kappa_{sm}}{2\zeta_s n_s}}{1 - i\frac{(n_a-n_s)\kappa_{sm}}{2\zeta_s n_s}}\right) + \frac{m\pi}{L} \quad (\text{S25a})$$

and $d_{sm} = \Delta_{sm}L/2\kappa_{sm}$, where:

$$\Delta_{sm} = \kappa_{sm} - \frac{m\pi}{L} \approx -\frac{m\pi}{L^2\zeta_s} \left[1 - \frac{1}{L\zeta_s} \left(1 - i\frac{n_a m\pi}{2n_s}\right)\right] \quad (\text{S26})$$

The d_{sm} parameter is a scattering length and for ideal cavity $\zeta_s \rightarrow \pm\infty$ goes to 0 because $\Delta_{sm} \rightarrow 0$, where Δ_{sm} denotes the difference between the ideal and non-ideal Fabry-Perot resonator. The ζ_s parameter is crucial in this approach as it defines the photon lifetime in the cavity and significantly influences the broadening of modes.

E. Hamiltonian

According to [6], we can define matrices $\mathbf{A}_1 = \mathbf{A} + \mathbf{A}^T$, $\mathbf{B}_1 = \mathbf{B} - \mathbf{A}^T\mathbf{A}$ and constant $\chi_{sm,s'm'} = c^2/2n_s n_{s'} \sqrt{\overset{\circ}{\omega}_{sm}(0)\overset{\circ}{\omega}_{s'm'}(0)}$. In this case, the approximated element of the multimode Hamiltonian is equal to:

$$\begin{aligned} \mathcal{H}_{sm,s'm'} &= \delta_{ss'} \delta_{mm'} \overset{\circ}{\omega}_{sm}(\mathbf{k}) + \\ &+ \chi_{sm,s'm'} (\mathbf{A}_1)_{ss'} Q_{sm,s'm'} + \\ &+ \chi_{sm,s'm'} \left(\mathbf{B}_1 - \frac{k_x^2 + k_y^2}{n_a^2} \mathbf{B}_0^0 - k_0^2 \mathbf{B}_0^1 \right)_{ss'} P_{sm,s'm'} \end{aligned} \quad (\text{S27})$$

where $P_{sm,s'm'}$ and $Q_{sm,s'm'}$ are equal to:

$$\begin{aligned} P_{sm,s'm'} &= \frac{n_s n_{s'}}{c^2} \int_0^L (\mathbf{E}_{sm}(z))^T \mathbf{E}_{s'm'}(z) dz \approx \\ &\approx \begin{cases} 0 & \text{if } m+m' \text{ odd,} \\ 1 & \text{if } m = m', \\ \frac{2L(m'\Delta_{sm} - m\Delta_{s'm'})}{\pi(m^2 - m'^2)} & \text{in other cases} \end{cases} \end{aligned} \quad (\text{S28a})$$

and

$$\begin{aligned} Q_{sm,s'm'} &= \frac{n_s n_{s'}}{c^2} \int_0^L (\mathbf{E}_{sm}(z))^T \partial_z \mathbf{E}_{s'm'}(z) dz \approx \\ &\approx \begin{cases} 0 & \text{if } m+m' \text{ even,} \\ \frac{4mm'}{L(m^2 - m'^2)} + \frac{8(m^3\Delta_{s'm'} - m'^3\Delta_{sm})}{\pi(m^2 - m'^2)^2} & \text{if } m+m' \text{ odd} \end{cases} \end{aligned} \quad (\text{S28b})$$

In this approach, we assumed that the modulation in the z direction is minimal, allowing us to treat each element of the matrices \mathbf{A}_1 , \mathbf{B}_1 , \mathbf{B}_0^0 and \mathbf{B}_0^1 as independent of the z coordinate. Consequently, these elements can be extracted from the integral and will be considered in further calculations as an 'effective value.' We postulate that each amplitude in the Fourier series for elements of the dielectric tensor, as defined in Eq. (S6), acts as a fitting parameter. Thus, we incorporate the z -direction dependence by adjusting the z -averaged effective amplitude values.

In the subsequent step, we simplify the multimode Hamiltonian to a 2-mode Hamiltonian, capturing the interaction between the nearest modes within the measurement range. Experimental data indicates the presence of a coupling between cavity modes of the same mode number, leading to the following formula for the 2×2 Hamiltonian matrix:

$$\mathcal{H}_{sm,s'm} = \delta_{ss'} \overset{\circ}{\omega}_{sm} + \chi_{sm,s'm} (\mathbf{B}_1 - k_0^2 \mathbf{B}_0^1)_{ss'} \quad (\text{S29})$$

where $\overset{\circ}{\omega}_{sm} = \kappa_{sm}c/n_s$. In the considered case, the component of the dielectric tensor depends on the position y , so in the 2-mode Hamiltonian there appears the product of an element of dielectric tensor and $k_y = -i\hbar\partial/\partial y$, so we have $k_y\varepsilon(y)$ and $k_y^2\varepsilon(y)$, which can be expressed in the symmetric form. The modulation $\hat{\varepsilon}$ in the z direction is low, so the electric field can be expressed as $\mathbf{E}_{sm}(y,z) = \mathbf{E}_{sm}(z) E_{sm}(y)$, where $E_{sm}(y)$ is a normalized periodic function with period d due to the periodicity of $\hat{\varepsilon}$. Using the above assumption we derived the formula for the element of the Hamiltonian matrix:

$$\begin{aligned} \mathcal{H}_{sm,s'm} &= \delta_{ss'} \overset{\circ}{\omega}_{sm} + \\ &+ \chi_{sm,s'm'} \langle E_{sm}(y) | (\mathbf{B}_1)_{ss'} | E_{s'm'}(y) \rangle - \\ &+ k_0^2 \chi_{sm,s'm'} \langle E_{sm}(y) | (\mathbf{B}_0^1)_{ss'} | E_{s'm'}(y) \rangle \end{aligned} \quad (\text{S30})$$

The first and third components are independent of the k_y and k_y^2 operators, so we applied the symmetrization procedure solely to the second term. This results in the

following form for the product of the derivative operator and the dielectric tensor:

$$\begin{aligned} & \langle E_{sm}(y) | \varepsilon_{1,ss'}(y) k_y | E_{s'm'}(y) \rangle = \\ & = -\frac{i}{2} \int_{-d/2}^{d/2} 2E_{sm}^*(y) \varepsilon_{1,ss'}(y) \frac{dE_{s'm'}(y)}{dy} dy + \\ & + E_{sm}^*(y) E_{s'm'}(y) \frac{d\varepsilon_{1,ss'}(y)}{dy} dy = \\ & = \langle E_{sm}(y) | \varepsilon_{1,ss'}(y) k_y | E_{s'm'}(y) \rangle^*, \quad (\text{S31a}) \end{aligned}$$

$$\begin{aligned} & \langle E_{sm}(y) | \varepsilon_{2,ss'}(y) k_y^2 | E_{s'm'}(y) \rangle = \\ & = -\int_{-d/2}^{d/2} E_{sm}^*(y) \frac{d\varepsilon_{2,ss'}(y)}{dy} \frac{dE_{s'm'}(y)}{dy} dy + \\ & + E_{sm}^*(y) \varepsilon_{2,ss'}(y) \frac{d^2 E_{s'm'}(y)}{dy^2} dy = \\ & = \langle E_{sm}(y) | \varepsilon_{2,ss'}(y) k_y^2 | E_{s'm'}(y) \rangle^* \quad (\text{S31b}) \end{aligned}$$

where $\varepsilon_{1,ss'}(y)$ and $\varepsilon_{2,ss'}(y)$ denote the ss' element of matrix \mathbf{B}_1 which is proportional to k_y and k_y^2 , respectively. The hermiticity of operators in Eq. (S31) can be proved by using integration by parts because the $E_{sm}(y)$ and $\varepsilon_{ss'}(y)$ are periodic function with period d .

F. Dispersion relation

Each element of the Hamiltonian matrix depends on the y coordinate because $\hat{\varepsilon}$ varies with it. To derive energy and polarization as functions of position in real space or wave vector in reciprocal space, we discretize the y coordinate. In this context, $k_y = -i\partial/\partial y$ and $k_y^2 = -\partial^2/\partial y^2$ are substituted by finite difference approximations, with the finite difference coefficients calculated as per Fornberg (1988) [7]. Diagonalizing this Hamiltonian yields $2N$ eigenvalues Λ (the set of all eigenvalues) and $2N$ eigenvectors Q (the set of all eigenvectors), where N represents the number of points in the lattice. Each eigenvector has $2N$ components, with the first N components corresponding to the amplitude as a function of position for horizontally polarized modes, and the second N for vertically polarized modes. The Stokes polarization parameters as functions of position and energy (in real space) were calculated using the following procedure:

$$\begin{aligned} S_{0,ij} &= \sum_{m=1}^N \sum_{n=1}^{2N} (|Q_{m,n}|^2 + |Q_{m+N,n}|^2) \cdot \\ & \cdot f_1(\text{Re}(E_n - E_i), \text{Im}(E_n)) f_2(y_j - y_m, \sigma), \quad (\text{S32a}) \end{aligned}$$

$$\begin{aligned} S_{1,ij} &= \sum_{m=1}^N \sum_{n=1}^{2p} (|Q_{m,n}|^2 - |Q_{m+N,n}|^2) \cdot \\ & \cdot f_1(\text{Re}(E_n - E_i), \text{Im}(E_n)) f_2(y_j - y_m, \sigma), \quad (\text{S32b}) \end{aligned}$$

TABLE I Parameters used in the simulation.

Parameter	value	Parameter	value
L	2.149 μm	d	6.5 μm
m_H	11	m_V	11
ζ_H	67 μm^{-1}	ζ_V	65 μm^{-1}
$\varepsilon_{xx,0}$	2.500	$\varepsilon_{yy,0}$	2.472
$\varepsilon_{xx,1}$	0.080	$\varepsilon_{yy,1}$	0.070
$\varepsilon_{xx,2}$	-0.025	$\varepsilon_{yy,2}$	-0.025
$\varepsilon_{xx,3}$	0.020	$\varepsilon_{yy,3}$	-0.015
$\varepsilon_{xx,4}$	-0.010	$\varepsilon_{yy,4}$	0.010
$\varepsilon_{zz,0}$	2.675	$\varepsilon_{zz,1}$	-0.150
$\varepsilon_{zz,2}$	0.050	$\varepsilon_{zz,3}$	-0.005
$\varepsilon_{xy,1}$	0.002 - 0.010 <i>i</i>	$\varepsilon_{yz,0}$	0.150
$\varepsilon_{yz,1}$	0.100	$\varepsilon_{xz,1}$	0.080 <i>i</i>
n_e	1.737	n_o	1.522

$$\begin{aligned} S_{2,ij} &= \sum_{m=1}^N \sum_{n=1}^{2p} (Q_{m+N,n}^* Q_{m,n} + Q_{m,n}^* Q_{m+N,n}) \cdot \\ & \cdot f_1(\text{Re}(E_n - E_i), \text{Im}(E_n)) f_2(y_j - y_m, \sigma), \quad (\text{S32c}) \end{aligned}$$

$$\begin{aligned} S_{3,ij} &= \sum_{m=1}^N \sum_{n=1}^{2p} i (Q_{m+N,n}^* Q_{m,n} - Q_{m,n}^* Q_{m+N,n}) \cdot \\ & \cdot f_1(\text{Re}(E_n - E_i), \text{Im}(E_n)) f_2(y_j - y_m, \sigma), \quad (\text{S32d}) \end{aligned}$$

where $S_{k,i,j}$ denote the value of k -th component of Stokes polarization parameters on the i, j position on the grid and f_1, f_2 are the Lorentz and Gaussian distributions:

$$f_1(x, \gamma) = \frac{1}{1 + x^2/\gamma^2} \quad (\text{S33a})$$

$$f_2(x, \sigma) = \exp\left(-\frac{x^2}{\sigma^2}\right) \quad (\text{S33b})$$

responsible for smoothing the solutions of discrete Hamiltonian.

The amplitude as a function of the wave vector for horizontally and vertically polarized modes was determined using the discrete Fourier transform. Given that the Hamiltonian comprises two subsets of modes, the Fourier transform was performed separately for each subset:

$$\tilde{Q}_{m,n} = \begin{cases} \sum_{k=1}^N Q_{k,n} e^{-2\pi i k m / N} & \text{if } m \leq N \\ \sum_{k=1}^N Q_{k+N,n} e^{-2\pi i k m / N} & \text{if } m > N \end{cases} \quad (\text{S34})$$

The Stokes polarization parameters as a function of energy and wave vector were calculated according to Eq. (S32), where Q and position y were replaced with \tilde{Q} and wave vector k , respectively.

G. Parameters in simulation

In our simulation's initial step, we estimate the cavity's thickness L , the number of modes (m_H and m_V),

and the linewidth ζ_H and ζ_V based on the modes' energy, as shown in Tab. I. Utilizing the nearly free electron model, we estimate the structure's period (d), consistent with real-space measurements. Next, we determine the amplitudes of $\varepsilon_{xx,n}$ and $\varepsilon_{yy,n}$ in Eq. (S6) to align each band's energy with the experimental data. The value of $\varepsilon_{zz,n}$ is selected to keep the $\hat{\varepsilon}$ matrix's trace constant in space, satisfying $\varepsilon_{zz,n} = -\varepsilon_{xx,n} - \varepsilon_{yy,n}$ for $n \neq 0$, and $\varepsilon_{zz,0} = 2n_o^2 + n_e^2 - \varepsilon_{xx,0} - \varepsilon_{yy,0}$ for $n = 0$, where n_o and n_e are the ordinary and extraordinary refractive indices for the liquid crystal, estimated from the data for E7 liquid crystal mixture presented in [8]. The value of $\varepsilon_{yz,0}$ comes from comparing the experimentally obtained and theoretically predicted effective mass for the vertically-polarized mode. The values of $\varepsilon_{xy,1}$, $\varepsilon_{xz,1}$, and $\varepsilon_{yz,1}$ are estimated by comparing the real and reciprocal space distribution of the Stokes polarization parameter S_2 and the reciprocal space's S_3 parameters. These sine components' values in-

dicating the strength of interband spin-orbit coupling. All $\varepsilon_{ij,n}$ values not listed in Tab. I are set to zero. Additionally, we assume a slightly non-perpendicular incident wave, setting $k_x = 1 \mu\text{m}^{-1}$. The polarization patterns in Fig. 3g-l of the main paper were derived using Eq. (S32) on a grid matching the measurements. The grid for the Hamiltonian with periodic boundary conditions consists of $N = 2^{10}$ points, with the simulation window ranging from $-60 \mu\text{m}$ to $60 \mu\text{m}$. Additionally, we carried out calculations for the Hamiltonian that accounts for interactions with other states: the 10th, 11th, and 12th horizontally and vertically polarized modes, as detailed in Eq. (S27). The results indicate that the polarization patterns in reciprocal and real space closely resemble those derived from the 2-mode Hamiltonian. This confirms the validity of simplifying the multimode Hamiltonian to a 2-mode Hamiltonian.

-
- [1] J. Martinand and G. Durand, Electric field quenching of thermal fluctuations of orientation in a nematic liquid crystal, *Solid State Commun.* **10**, 815 (1972).
- [2] P. Rudquist, L. Komitov, and S. Lagerwall, Linear electro-optic effect in a cholesteric liquid crystal, *Phys. Rev. E* **50**, 4735 (1994).
- [3] P.-G. De Gennes and J. Prost, *The physics of liquid crystals*, 83 (Oxford University Press, 1993).
- [4] Z. Jia, T. Pawale, G. I. Guerrero-García, S. Hashemi, J. A. Martínez-González, and X. Li, Engineering the uniform lying helical structure in chiral nematic liquid crystals: From morphology transition to dimension control, *Crystals* **11**, 414 (2021).
- [5] P. Oswald, J. Baudry, and S. Pirkl, Static and dynamic properties of cholesteric fingers in electric field, *Physics Reports* **337**, 67 (2000).
- [6] P. Oliwa, W. Bardyszewski, and J. Szczytko, Quantum mechanical-like approach with non-hermitian effective hamiltonians in spin-orbit coupled optical cavities, *Phys. Rev. Res.* **6**, 013324 (2024).
- [7] B. Fornberg, Generation of finite difference formulas on arbitrarily spaced grids, *Mathematics of Computation* **51**, 699 (1988).
- [8] J. Li, C.-H. Wen, S. Gauza, R. Lu, and S.-T. Wu, Refractive indices of liquid crystals for display applications, *Journal of Display Technology* **1**, 51 (2005).